LETTERS

Haem homeostasis is regulated by the conserved and concerted functions of HRG-1 proteins

Abbhirami Rajagopal[1], Anita U. Rao[1], Julio Amigo[2], Meng Tian[3], Sanjeev K. Upadhyay[4], Caitlin Hall[1], Suji Uhm[1], M. K. Mathew[4], Mark D. Fleming[3], Barry H. Paw[2], Michael Krause[5] & Iqbal Hamza[1]

Haems are metalloporphyrins that serve as prosthetic groups for various biological processes including respiration, gas sensing, xenobiotic detoxification, cell differentiation, circadian clock control, metabolic reprogramming and microRNA processing[1–4]. With a few exceptions, haem is synthesized by a multistep biosynthetic pathway comprising defined intermediates that are highly conserved throughout evolution[5]. Despite our extensive knowledge of haem biosynthesis and degradation, the cellular pathways and molecules that mediate intracellular haem trafficking are unknown. The experimental setback in identifying haem trafficking pathways has been the inability to dissociate the highly regulated cellular synthesis and degradation of haem from intracellular trafficking events[6]. *Caenorhabditis elegans* and related helminths are natural haem auxotrophs that acquire environmental haem for incorporation into haemoproteins, which have vertebrate orthologues[7]. Here we show, by exploiting this auxotrophy to identify HRG-1 proteins in *C. elegans*, that these proteins are essential for haem homeostasis and normal development in worms and vertebrates. Depletion of *hrg-1*, or its paralogue *hrg-4*, in worms results in the disruption of organismal haem sensing and an abnormal response to haem analogues. HRG-1 and HRG-4 are previously unknown transmembrane proteins, which reside in distinct intracellular compartments. Transient knockdown of *hrg-1* in zebrafish leads to hydrocephalus, yolk tube malformations and, most strikingly, profound defects in erythropoiesis—phenotypes that are fully rescued by worm HRG-1. Human and worm proteins localize together, and bind and transport haem, thus establishing an evolutionarily conserved function for HRG-1. These findings reveal conserved pathways for cellular haem trafficking in animals that define the model for eukaryotic haem transport. Thus, uncovering the mechanisms of haem transport in *C. elegans* may provide insights into human disorders of haem metabolism and reveal new drug targets for developing anthelminthics to combat worm infestations.

In animals, the terminal enzyme in haem synthesis, ferrochelatase, is located on the matrix side of the inner mitochondrial membrane[8]. Most newly synthesized haem must be transported through mitochondrial membranes to haemoproteins found in distinct intracellular membrane compartments[6]. Haem synthesis is regulated at multiple steps by effectors including iron, haem and oxygen to prevent the uncoordinated accumulation of haem or its precursors[5]. *C. elegans* is a haem auxotroph and is therefore a unique genetic animal model in which to identify the molecules and delineate the cellular pathways for eukaryotic haem transport[6]. Haem analogue studies have suggested that a haem uptake system exists in *C. elegans*[7]. Synchronized *C. elegans* cultures grown in axenic mCeHR-2 liquid medium[9] and supplemented with haemin chloride revealed a robust uptake of fluorescent zinc mesoporphyrin IX (ZnMP) at a haem concentration of 20 μM or less, in contrast with worms grown at 100 μM haem or more (Fig. 1a, b), suggesting that the transport and accumulation of haem are regulated.

We conducted genome-wide microarrays to identify genes that are transcriptionally regulated by haem. Wild-type N2 worms were grown for two synchronized generations in 4 μM (low), 20 μM (optimal) and 500 μM (high) haem concentrations in liquid medium and their messenger RNA was hybridized to Affymetrix *C. elegans* genome arrays. Statistical analyses identified changes in 370 genes, of which about 164 had some sequence identity to genes in the human genome databases at the amino-acid level, and more than 90% of the genes had no functional annotation in the *C. elegans* database (Supplementary Table 1).

We postulated that the expression of genes that encode for haem transporters might be elevated during haem deficiency to maximize uptake of dietary haem. To identify candidate haem transporter genes, we sorted the 117 genes to identify those that were specifically upregulated in low haem (Supplementary Table 1, categories 1 and 2) and encoded for proteins with predicted transmembrane domains, transport functions, and/or haem/metal-binding motifs. F36H1.5 was >10-fold upregulated at low haem but was undetectable at 500 μM haem, and the predicted open reading frame of 169 amino acids (≈19 kDa) showed similarities to high-affinity permease transporters[10]. We refer to F36H1.5 as haem responsive gene-4 (*hrg-4*). RNA blotting and qRT–PCR analysis revealed that *hrg-4* mRNA was significantly upregulated (>40-fold) at 4 μM haem but undetectable at 20 and 500 μM haem (Fig. 1c, d). We identified three putative paralogues of *hrg-4* in the *C. elegans* genome; we termed them *hrg-1* (R02E12.6), *hrg-5* (F36H1.9) and *hrg-6* (F36H1.10), with 27%, 39% and 35% overall amino-acid sequence identity, respectively (Fig. 1e and Supplementary Fig. 1a). Although both *hrg-1* and *hrg-4* were highly responsive to haem deficiency (Fig. 1c), the magnitude of change in mRNA expression at 1.5 μM haem and their responsiveness to haem-mediated repression were markedly different (Fig. 1d and inset). By contrast, *hrg-5* and *hrg-6* expression seemed to be constitutive and not regulated by haem (not shown). *hrg-4*, *hrg-5* and *hrg-6* are nematode-specific genes, whereas *hrg-1* has orthologues with about 25% amino acid identity in vertebrates (Fig. 1e, f, and Supplementary Fig. 1). Topology modelling and motif analysis of HRG-1 identified four predicted transmembrane domains (TMDs) and a conserved tyrosine and acidic-dileucine-based sorting signal in the cytoplasmic carboxy terminus (Fig. 1e and Supplementary Fig. 1a)[11]. In addition, residues that could potentially either directly bind haem (H90 in TMD2) or interact with the

[1]Department of Animal & Avian Sciences and Department of Cell Biology & Molecular Genetics, University of Maryland, College Park, Maryland 20742, USA. [2]Division of Hematology, Department of Medicine, Brigham and Women's Hospital, Harvard Medical School, Boston, Massachusetts 02115, USA. [3]Department of Pathology, Children's Hospital Boston, Boston, Massachusetts 02115, USA. [4]National Centre for Biological Sciences, Tata Institute of Fundamental Research, UAS-GKVK campus, Bangalore 560 065, India. [5]Laboratory of Molecular Biology, National Institute of Diabetes and Digestive and Kidney Diseases, National Institutes of Health, Bethesda, Maryland 20892, USA.

haem side chains (FARKY) were situated in the C-terminal tail (Fig. 1e, g)[12–14].

To study the function of *hrg-1* genes in haem homeostasis, we generated a *hrg-1::gfp* transcriptional fusion in *C. elegans*. *hrg-1::gfp* was expressed specifically in the intestinal cells in larvae and adults (Fig. 2a). Its expression was regulated by feeding transgenic worms sequentially with *Escherichia coli* that had been grown on agar plates with or without exogenous haem (Fig. 2a). *hrg-1* repression was specific to haem because neither protoporphyrin IX nor iron altered the expression of *hrg-1::gfp* (Fig. 2b). We next assessed the effect of HRG-1 and HRG-4 depletion in worms by RNA-mediated interference with three independent assays: first, the expression of green fluorescent protein (GFP) in the *hrg-1::gfp* haem sensor strain to monitor haem homeostasis; second, the accumulation of fluorescent ZnMP as a function of haem uptake; and third, animal viability in the presence of a cytotoxic haem analogue, gallium protoporphyrin IX (GaPP)[7]. Knockdown of *hrg-4* by RNAi resulted in the expression of *hrg-1::gfp*, even though haem levels sufficient to suppress GFP were present in the diet (Fig. 2c). *hrg-4* RNAi resulted in no detectable accumulation of ZnMP fluorescence in worms that were grown in 1.5 μM haem, a concentration that is sufficient to induce a robust uptake of haem (Fig. 2d). Consistent with these findings was our observation that progeny from *hrg-4* RNAi worms were also markedly resistant to GaPP toxicity (Fig. 2e), in concordance with recent genome-wide studies revealing *hrg-4* expression in the worm intestine[15]. In contrast, *hrg-1* RNAi showed a significant derepression of GFP only at low haem levels in the *hrg-1::gfp* haem sensor strain (Fig. 2c), but no discernible effect on animal viability assessed with GaPP toxicity assays (Fig. 2e). We found that the intensity of ZnMP fluorescence was significantly greater in the intestines of HRG-1-depleted worms than in controls (Fig. 2d and Supplementary Fig. 2). The observed differences in RNAi phenotypes of *hrg-4* and *hrg-1* suggest that haem uptake into worm intestinal cells involves HRG-4, whereas HRG-1 mediates haem homeostasis by means of an intracellular compartment.

To dissect HRG-1 function in a vertebrate genetic model, we used zebrafish (*Danio rerio*). We reasoned that any perturbation in haem homeostasis would be manifested as haematological defects in the fish embryo[16]. BLAST searches revealed an orthologous gene on zebrafish chromosome 6 that shared about 21% amino acid identity with *C. elegans* HRG-1. Whole-mount *in situ* hybridization of zebrafish embryos at the 15-somite stage and 24 h after fertilization showed zebrafish *hrg-1* mRNA expressed throughout the embryo, including the central nervous system (Fig. 3a). To knock down *hrg-1* in zebrafish, antisense morpholinos (MO2) were designed at the splice junctions to selectively induce *hrg-1* mRNA mis-splicing and degradation. Embryos injected with MO2 had severe anaemia and lacked any detectable *o*-dianisidine-positive erythroid cells (Fig. 3b, c). MO2 morphants showed other developmental defects, including hydrocephalus and a curved body with shortened yolk tube.

The phenotypes observed in *hrg-1* knockdown embryos suggested an essential role for zebrafish *hrg-1* in the specification, maintenance or maturation of the erythroid cell lineage. *hrg-1* morphants revealed wild-type levels of *βe1*−globin mRNA, a marker for haemoglobinization in the developing blood island and intermediate cell mass of embryos at 24 h after fertilization, but by 48 h after fertilization there were no detectable globin-producing cells (Supplementary Fig. 3a).

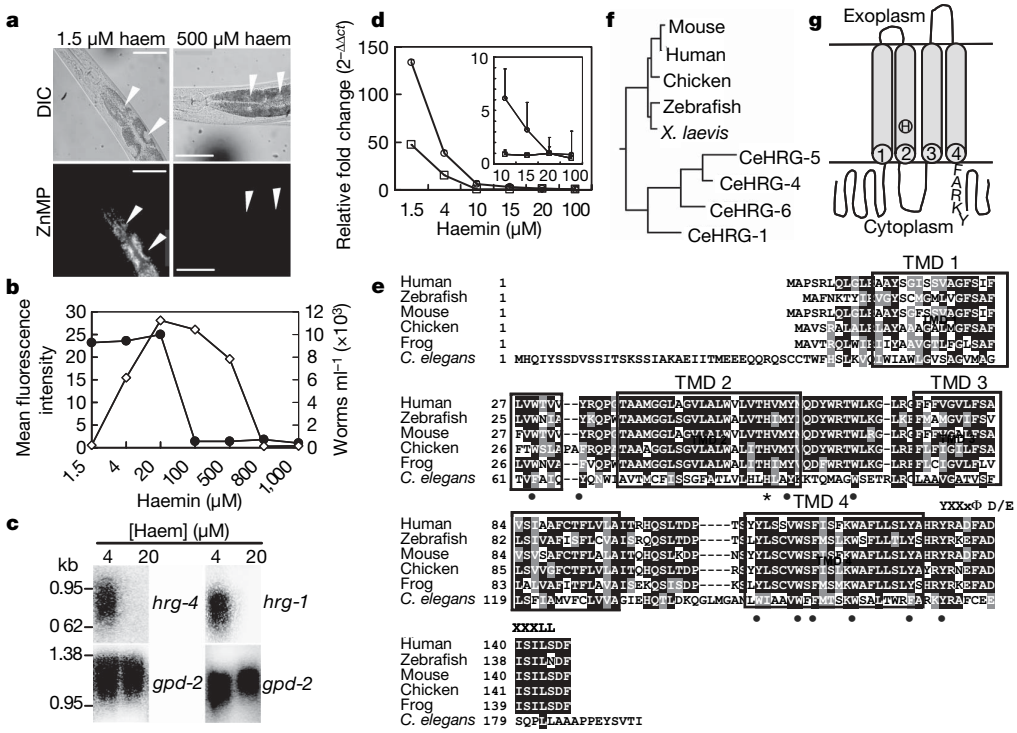

Figure 1 | Identification of *hrg-1* and *hrg-4* in *C. elegans*. **a**, Fluorescent ZnMP (40 μM for 3 h) accumulation in worms grown in mCeHR-2 medium supplemented with 1.5 μM (left) and 500 μM (right) haem. Differential interference contrast (DIC, top) and rhodamine fluorescence (bottom). **b**, Total mean fluorescence intensity (filled circles) of ZnMP accumulated in worms (40 μM for 3 h) after 9 days of growth in mCeHR-2 medium supplemented with the indicated haem concentrations. Open diamonds, growth of worms in haemin. Results are means ± s.d. ($n = 100$). **c**, Northern blot analysis of *hrg-1* and *hrg-4* expression in response to 4 and 20 μM haem in mCeHR-2 medium. The blot was stripped and reprobed with glyceraldehyde 3-phosphate dehydrogenase (*gpd-2*) as loading control. kb, kilobases. **d**, Expression of *hrg-4* (circles) and *hrg-1* (squares) mRNA estimated by quantitative RT–PCR from total RNA obtained from worms grown at the indicated haem concentrations. Each data point shows mean ± s.d. and the results are representative of three separate experiments. Inset: mRNA levels at higher haem concentrations. **e**, Multiple sequence alignment of *C. elegans* HRG-1 with its vertebrate orthologues. Asterisk, histidine (H90); circles, aromatic amino acids; box, putative transmembrane domains; YXXxϕ, C-terminal tyrosine motif; D/EXXxLL, di-leucine motif. **f**, Phylogenetic analysis of HRG-1 proteins using the neighbour-joining method. **g**, Predicted topology of *C. elegans* HRG-1 showing H90 in TMD2, and FARKY, the putative haem-interacting motif, in the cytoplasmic tail.

Moreover, markers for myeloid (*MPO* and *L-plastin*) and thrombocyte (platelet-equivalent, *cd41*) lineages were normal in the *hrg-1* morphant embryos (Supplementary Fig. 3b, c)[17,18]. These findings indicate that zebrafish *hrg-1* is not required for cell lineage specification but rather for maintenance and haemoglobinization of the embryonic erythroid cells. Similarly, *pax 2.1* mRNA expression, a marker of the midbrain/hindbrain boundary organizer, was severely deficient in the central nervous system of MO2 morphants, indicating that midbrain–hindbrain development in zebrafish is also dependent on *hrg-1* (Supplementary Fig. 3d). To verify whether the knockdown phenotypes observed in zebrafish corresponded functionally to the RNAi phenotypes in *C. elegans* (compare Fig. 2c–e with Fig. 3b, c), we co-injected MO2 in the presence and absence of *C. elegans hrg-1* synthetic antisense RNA (cRNA). Despite the modest (21%) sequence identity between the *C. elegans* and zebrafish HRG-1, more than 85% of the morphant embryos were fully rescued by *Cehrg-1* (95 of 108 mutants rescued), in contrast with none for the control embryos (0 of 194 mutants rescued), correcting the defects in anaemia, hydrocephalus and body axis curvature (Fig. 3d, e). These studies suggest that *C. elegans* and zebrafish HRG-1 have a highly conserved function in modulating haem homeostasis.

To dissect the function of HRG-1 in vertebrates further, we examined its gene expression, intracellular localization and biochemical properties in mammalian cells. Genome database searches with *C. elegans* HRG-1 identified an orthologous gene, which we refer to as *hHRG-1* (Fig. 1e), with about 23% and 65% identity to worm and zebrafish HRG-1 proteins, respectively. *hHRG-1* is located on human chromosome 12q13, about 3.2 megabases from *DMT1*, a gene encoding the main iron transporter in mammals[19,20]. RNA blotting of human adult tissues and tumour cell lines detected two *hHRG-1* transcripts about 1.7 and 3.1 kilobases long, with the shorter form predominant (Fig. 4a, b). *hHRG-1* was highly expressed in the brain, kidney, heart and skeletal muscle (Fig. 4a and Supplementary Fig. 4a), and moderately expressed in the liver, lung, placenta and small intestine. *hHRG-1* was abundantly expressed in cell lines derived from duodenum (HuTu 80), kidney (ACHN, HEK-293), bone marrow (HEL, K562) and brain (M17, SH-SY5Y) (Fig. 4b and Supplementary Fig. 4b). Neither altering cellular haem and iron status nor chemically inducing Friend mouse erythroleukaemia (MEL) cells to produce haemoglobin altered *HRG-1* at the transcriptional level in mammalian cells (Supplementary Fig. 5). However, our findings do not exclude the possibility that HRG-1 may be regulated at the post-translational level.

To assess the localization and function of HRG-1 protein, *C. elegans* (Ce)HRG-1, hHRG-1 and CeHRG-4 were tagged at the C terminus with either the haemagglutinin (HA) epitope or GFP variants and transiently transfected into HEK-293 cell lines. All three proteins migrated as a monomer as well as more slowly migrating oligomers (Fig. 4c, lanes 1–6). The oligomerization did not occur in solution after cell lysis or because of protein overexpression, because *in vitro* transcription and translation revealed a single main radiolabelled band corresponding to the monomer for each protein (Fig. 4c, lanes 7–9). Confocal microscopy studies with cells expressing fluorescently tagged proteins showed HRG-4 clearly on the periphery of cells and localized together with a plasma membrane marker. In contrast, CeHRG-1 and hHRG-1 were distributed in an intracellular compartment punctuated throughout the cytoplasm, with about 10% of the total fluorescence on the cell periphery (Fig. 4d). Co-expression of CeHRG-1 and hHRG-1 in the same cell resulted in more than 80% of the two proteins being localized to the same intracellular sites (Fig. 4d). Confocal studies with cellular organelle markers localized CeHRG-1 and hHRG-1 together with LAMP1 (more than 90%), and partly with rab 7 and rab 11 (about 50–70%; Supplementary Fig. 6). These results suggest that HRG-1 proteins are located primarily in endosomes and lysosome-related organelles and are consistent with the presence of sorting motifs in HRG-1 (Fig. 1e)[11].

The presence of conserved haem-binding amino-acid residues in conjunction with the haem-dependent RNAi phenotype in *C. elegans* implied that HRG-1 and HRG-4 may interact with haem. Haemin-agarose affinity chromatography performed on cell lysates from transiently transfected HEK-293 cells showed significant binding of CeHRG-4, CeHRG-1 and hHRG-1 to haem (Fig. 4e), whereas little binding was observed for human ZIP4, an eight-transmembrane-domain zinc transporter that localizes to the plasma membrane and perinuclear cytoplasmic vesicles[21]. Because HRG-1 localized to endosomal–lysosomal organelles whereas HRG-4 is on the plasma

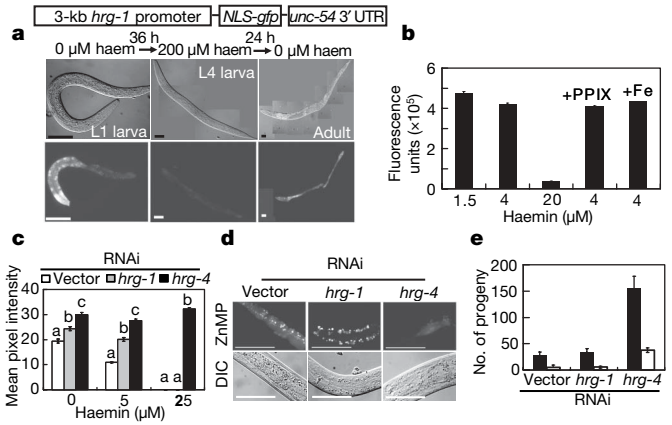

Figure 2 | *hrg-1* and *hrg-4* are essential for haem homeostasis in *C. elegans*. **a**, IQ6011 *hrg-1::gfp* 'haem sensor' strain responds to exogenous haem after sequential exposure to *E. coli* grown on agar plates in the absence (left and right) and presence (middle) of 200 μM haem. UTR, untranslated region. **b**, Spectrofluorometric measurements of GFP in worm lysates from IQ6011 strain grown in the presence of indicated concentrations of haem plus 20 μM protoporphyrin IX (PPIX) or 1 mM $FeCl_3$. Each data point shows mean ± s.d. and the results are representative of three separate experiments. **c–e**, Depletion of *hrg-1* or *hrg-4* in worms by RNAi with feeding bacteria. **c**, Dysregulation of GFP (means ± s.e.m.; $n = 35–45$ worms per treatment) in IQ6011 when fed with bacteria grown in the presence of 0, 5 and 25 μM haem. Values with different letter labels are significantly different ($P < 0.001$) within each treatment. **d**, Aberrant ZnMP fluorescence accumulation in worms fed with 10 μM ZnMP for 16 h. Scale bar, 50 μm. **e**, Differences in viable progeny (mean ± s.d.; $n = 30$ P_0 worms per treatment) after 5 days of exposure to 1 μM GaPP plus RNAi bacteria. Filled bars, viable eggs; open bars, larvae. The results for **c–e** are representative of at least four separate experiments.

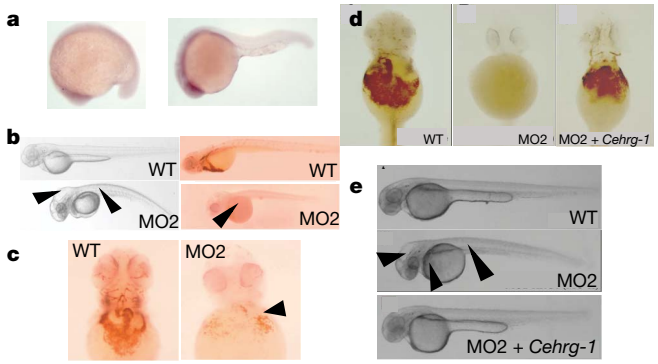

Figure 3 | HRG-1 is essential for erythropoiesis and development in zebrafish. **a**, Zebrafish *hrg-1* expression by whole-mount *in situ* hybridization: left, 15 somites; right, 24 h after fertilization. **b**, Knockdown of zebrafish *hrg-1* by using morpholinos (MO2) against zebrafish *hrg-1* reveals severe anaemia with very few *o*-dianisidine-positive red cells (arrows, right panel), hydrocephalus, and a curved body with shortened yolk tube (arrows, left panel). WT, wild type. **c**, Decrease in haemoglobinized cells in MO2 morphants (arrows). **d**, **e**, *Cehrg-1* cRNA injected along with MO2, shows restoration of haemoglobinized cells (**d**) and complete rescue of the developmental defects of hydrocephalus, body axis curvature, and yolk sac formation (**e**, arrows).

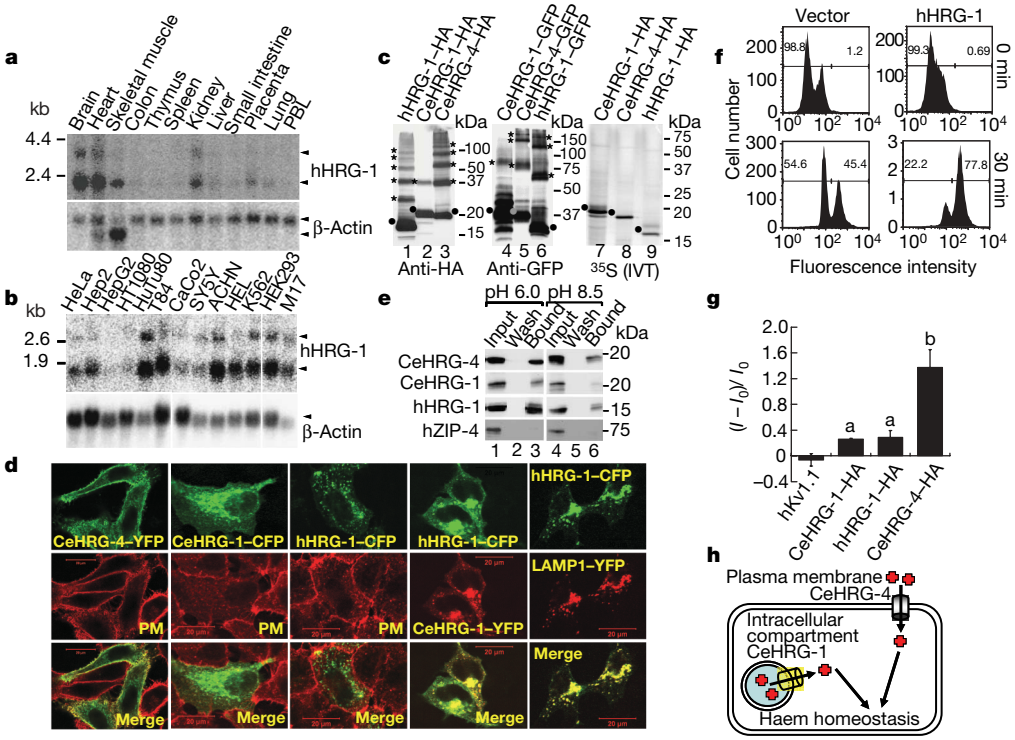

Figure 4 | Expression, localization and functional studies of worm and mammalian *hrg-1*. **a**, **b**, mRNA expression of human HRG-1 in multiple adult human tissues (**a**; PBL, peripheral blood leukocytes) and human tissue-derived cell lines (**b**). The blots were stripped and reprobed with β-actin as loading control. **c**, Expression of C-terminally tagged proteins in transfected HEK-293 cells by SDS–PAGE and immunoblotting with antibodies against HA (lanes 1–3, 50 μg) and GFP (lanes 4–6, 25 μg), or by *in vitro* expression with ^{35}S fluorography (lanes 7–9, one-fifth of total extract). **d**, Cellular localization of C-terminally tagged fluorescent proteins in transfected HEK-293 cells by confocal microscopy. The plasma membrane (PM) was identified using wheatgerm agglutinin. Scale bar, 20 μm. **e**, HRG-1 proteins interact with haem as a function of pH. Cell lysates (lanes 1 and 4, one-tenth of total protein) from HEK-293 cells expressing the indicated HA-tagged proteins were incubated with haemin-agarose. Wash (lanes 2 and 5) depicts the final wash before elution of the bound protein (lanes 3 and 6) from the haemin-agarose column. Samples were subjected to SDS–PAGE followed by immunoblotting with anti-HA antisera. **f**, Flow-cytometry histograms show enhanced ZnMP uptake and accumulation after 30 min of incubation with 5 μM ZnMP in MEL cells stably expressing either hHRG-1–HA (right) or empty vector (left). **g**, Electrophysiological currents (means ± s.d., $n = 4$) elicited from *Xenopus* oocytes injected with cRNA encoding the indicated protein, when clamped at −110 mV in the presence of 20 μM haemin chloride. The *y* axis represents the difference in current in the presence and absence of haemin, normalized to the current observed in the absence of haem. Values with different letter labels are significantly different ($P < 0.05$) within each treatment compared with hKv1.1 control. **h**, Proposed model for the function of HRG-1 proteins in haem homeostasis in *C. elegans* intestinal cells. CeHRG-4 mediates haem uptake through the plasma membrane, whereas CeHRG-1 facilitates intracellular haem availability through an endosomal and/or lysosomal-related compartment. The model does not exclude the possibilities that CeHRG-1 traffics through the plasma membrane and may be functional on the cell surface.

membrane, we reasoned that these proteins may bind haem as a function of pH. In a manner consistent with their localization, haem binding to HRG-1 was significantly decreased by increasing the pH, in contrast with HRG-4, which bound haem over a broader pH range (Fig. 4e, lanes 3 and 6). These binding assays, together with the intracellular localization results, correlate directly with the phenotypic differences observed in worms in which *hrg-1* and *hrg-4* were knocked down by RNAi (Fig. 2c–e).

We next investigated whether HRG-1 proteins mediate haem uptake, by expressing *hHRG-1* ectopically in MEL cells. ZnMP uptake or retention was substantially altered in MEL cells constitutively expressing *hHRG-1* in comparison with control cells; maximal differences were observed after 30 min of incubation (Fig. 4f and Supplementary Fig. 7). To assay haem transport directly, *Xenopus laevis* oocytes were injected with cRNA and haem-dependent currents were monitored under a two-electrode voltage clamp. Significant inward currents of over 250 nA were observed when 20 μM haem was added to oocytes clamped at −110 mV and injected with cRNA for CeHRG-1, hHRG-1 and CeHRG-4; this is indicative of haem-dependent transport across the plasma membrane (Fig. 4g and Supplementary Fig. 8). Together, these results show that the worm and mammalian HRG-1 proteins transport haem.

Given the parallels between copper, iron and haem in their biochemical reactivity and toxicity, we envisage an intricate cellular network of haem homeostasis molecules that bind, transfer and compartmentalize haem[6,22,23]. We propose a model of haem homeostasis in which CeHRG-4 mediates haem uptake in *C. elegans* at the plasma membrane, whereas CeHRG-1 regulates intracellular haem availability through an endosomal compartment (Fig. 4h). Haem limitation would induce the uptake and regulated sequestration of an essential, but toxic, macrocycle by the coordinated actions of CeHRG-4 and CeHRG-1 functioning in distinct membrane compartments. Because haems have greater solubility below or above physiological pH, compartmentalization of HRG-1 to an acidic endosome or a lysosome-related organelle would permit haem to remain soluble. The presence of HRG-1 in both *C. elegans* and vertebrates suggests that the components for intracellular regulation and movement of haem by means of HRG-1 are conserved in metazoans.

METHODS SUMMARY

C. elegans strains were grown either in liquid mCeHR-2 medium or on Nematode Growth Medium agar plates spotted with *E. coli*. Cell lines were routinely cultured in basal growth medium composed of DMEM and 10% bovine serum. We maintained zebrafish on a standard genetic AB or Tü wild-type background. For microarray analysis, synchronized F_2 larvae were re-inoculated in mCeHR-2 medium supplemented with 4, 20 or 500 μM haemin and harvested at the late L4 stage for hybridization to a Affymetrix *C. elegans* Whole Genome Array. *C. elegans hrg-1* putative promoter was cloned into pPD95.67 to create a *hrg-1::gfp* transcriptional fusion (strain IQ6011). For

RNAi experiments, equal numbers of IQ6011 synchronized F_1 L1 larvae were placed on NGM agar plates containing 2 mM isopropyl β-D-thiogalactoside and spotted with RNAi feeding bacteria that had been grown in Luria–Bertani broth supplemented or not with haemin for 5.5 h. For GFP measurements, worms were harvested and lysed to quantify GFP fluorescence with an ISS PC1 spectrofluorimeter. Pull-down assays of transfected HEK-293 cells were performed with equivalent amounts of target protein and 300 nmol of haemin-agarose. For confocal microscopy studies, a Zeiss laser scanning LSM 510 equipped with argon and HeNe lasers was used. For zebrafish experiments, whole-mount *in situ* hybridization was performed with digoxigenin-labelled cRNA probes in accordance with standard protocols. Live embryos at 48–72 h after fertilization were stained for haemoglobinized cells with *o*-dianisidine. Zebrafish *hrg-1* gene rescue assays were performed by injecting 1.5 ng of MO2 morpholino together with 200 pg of *C. elegans hrg-1* cRNA. For flow cytometry, MEL cells stably expressing HRG-1 were incubated with 5 μM ZnMP and the fluorescence intensity was measured by flow cytometry. Electrophysiological measurements in *Xenopus* oocytes injected with cRNA were performed with a two-electrode voltage clamp.

Received 19 September 2007; accepted 31 March 2008.
Published online 16 April 2008.

1. Ponka, P. Cell biology of heme. *Am. J. Med. Sci.* **318,** 241–256 (1999).
2. Kaasik, K. & Lee, C. C. Reciprocal regulation of haem biosynthesis and the circadian clock in mammals. *Nature* **430,** 467–471 (2004).
3. Yin, L. *et al.* Rev-erbα, a heme sensor that coordinates metabolic and circadian pathways. *Science* **318,** 1786–1789 (2007).
4. Faller, M. *et al.* Heme is involved in microRNA processing. *Nature Struct. Mol. Biol.* **14,** 23–29 (2007).
5. Medlock, A. E. & Dailey, H. A. in *Tetrapyrroles* (eds Warren, M. & Smith, A. G.) 116–127 (Landes Bioscience and Springer Science + Business Media, Austin, TX, 2007).
6. Hamza, I. Intracellular trafficking of porphyrins. *Am. Chem. Soc. Chem. Biol.* **1,** 627–629 (2006).
7. Rao, A. U., Carta, L. K., Lesuisse, E. & Hamza, I. Lack of heme synthesis in a free-living eukaryote. *Proc. Natl Acad. Sci. USA* **102,** 4270–4275 (2005).
8. Dailey, H. A. Terminal steps of haem biosynthesis. *Biochem. Soc. Trans.* **30,** 590–595 (2002).
9. Nass, R. & Hamza, I. in *Current Protocols in Toxicology* (eds Maines, M. D. *et al.*) 1.9.1–1.9.17 (Wiley, New York, 2007).
10. Kanehisa, M. *et al.* From genomics to chemical genomics: new developments in KEGG. *Nucleic Acids Res.* **34,** D354–D357 (2006).
11. Bonifacino, J. S. & Traub, L. M. Signals for sorting of transmembrane proteins to endosomes and lysosomes. *Annu. Rev. Biochem.* **72,** 395–447 (2003).
12. Schmidt, P. M. *et al.* Residues stabilizing the heme moiety of the nitric oxide sensor soluble guanylate cyclase. *Eur. J. Pharmacol.* **513,** 67–74 (2005).
13. Pellicena, P. *et al.* Crystal structure of an oxygen-binding heme domain related to soluble guanylate cyclases. *Proc. Natl Acad. Sci. USA* **101,** 12854–12859 (2004).
14. Goldman, B. S., Beck, D. L., Monika, E. M. & Kranz, R. G. Transmembrane heme delivery systems. *Proc. Natl Acad. Sci. USA* **95,** 5003–5008 (1998).
15. McGhee, J. D. *et al.* The ELT-2 GATA-factor and the global regulation of transcription in the *C. elegans* intestine. *Dev. Biol.* **302,** 627–645 (2007).
16. Shafizadeh, E. & Paw, B. H. Zebrafish as a model of human hematologic disorders. *Curr. Opin. Hematol.* **11,** 255–261 (2004).
17. Bennett, C. M. *et al.* Myelopoiesis in the zebrafish, *Danio rerio*. *Blood* **98,** 643–651 (2001).
18. Lin, H. F. *et al.* Analysis of thrombocyte development in CD41-GFP transgenic zebrafish. *Blood* **106,** 3803–3810 (2005).
19. Fleming, M. D. *et al.* Microcytic anaemia mice have a mutation in *Nramp2*, a candidate iron transporter gene. *Nature Genet.* **16,** 383–386 (1997).
20. Gunshin, H. *et al.* Cloning and characterization of a mammalian proton-coupled metal-ion transporter. *Nature* **388,** 482–488 (1997).
21. Mao, X. *et al.* A histidine-rich cluster mediates the ubiquitination and degradation of the human zinc transporter, hZIP4, and protects against zinc cytotoxicity. *J. Biol. Chem.* **282,** 6992–7000 (2007).
22. Rees, E. M. & Thiele, D. J. From aging to virulence: forging connections through the study of copper homeostasis in eukaryotic microorganisms. *Curr. Opin. Microbiol.* **7,** 175–184 (2004).
23. De Domenico, I., McVey Ward, D. & Kaplan, J. Regulation of iron acquisition and storage: consequences for iron-linked disorders. *Nature Rev. Mol. Cell Biol.* **9,** 72–81 (2008).

Supplementary Information is linked to the online version of the paper at www.nature.com/nature.

Acknowledgements The Hamza laboratory thanks the DC-Baltimore WormClub for advice and criticism. We also thank P. Aplan, H. Dailey, I. Mather and S. Severance for critical discussions and reading of the manuscript; M. Cam and G. Poy for expertise with microarrays; J. Lippincott-Schwartz and D. Hailey for organelle markers; H.-F. Lin and R. Handin for the Tg(CD41–GFP) transgenic zebrafish line; J. Italiano for use of the Orca IIER charge-coupled device camera/Metamorph software; P. Krieg for the pT7TS *Xenopus* oocyte expression vector; P. Ponka and R. Eisenstein for the SIH iron chelation; D. Beckett for use of the fluorescent spectrophotometer; and M. Petris for the hZIP4 plasmid. Many of the worm strains were provided by the *Caenorhabditis* Genetics Center. This work was supported by funding from the National Institutes of Health (NIH) (I.H., M.D.F. and B.H.P.), the March of Dimes Birth Defects Foundation (I.H. and B.H.P.), the NIH/National Institute of Diabetes and Digestive and Kidney Diseases Intramural Research Program (M.K.), Council for Scientific and Industrial Research and Kanwal Rekhi Fellowships (S.K.U.), and a Howard Hughes Medical Institute Undergraduate Science Education Program grant (S.U.).

Author Contributions Experimental design and execution were as follows: worm experiments and microarrays, A.R., A.U.R., M.K. and I.H.; mammalian experiments, A.R., A.U.R., M.T., C.H., S.U., M.D.F. and I.H.; zebrafish experiments, J.A. and B.H.P.; *Xenopus* injections and measurements, S.K.U. and M.K.M. I.H. wrote the manuscript. All authors discussed the results and commented on the manuscript.

Author Information The microarray data have been deposited with the Gene Expression Omnibus at NCBI under accession number GSE8696. Reprints and permissions information is available at www.nature.com/reprints. Correspondence and requests for materials should be addressed to I.H. (hamza@umd.edu).

SUPPLEMENTARY INFORMATION

Supplementary Figures and Legends

Tables

Table S1: Summary of the 370 heme-responsive genes identified using Affymetrix *C. elegans* whole genome microarrays.

Figures

Fig. S1: Sequence analysis of HRG-1 proteins. ***(a)*** Multiple sequence alignment of CeHRG-1, -4, -5 and -6 paralogs obtained using ClustalW (v. 1.83). Identical amino acids and conservative changes are indicated by reversed and shaded characters, respectively. Boxed residues denote the four putative transmembrane domains based on predictions from HRG-1. C-terminus tyrosine (Yxxϕ) and di-leucine (D/ExxxLL) based sorting motifs in HRG-1 are indicated. Notably, HRG-4 lacks both sorting signals and residue H90 (asterisk) in TMD2 is substituted with a tyrosine (Y63). Unlike histidines, tyrosine heme ligands have a lower redox potential and the coordination stabilizes heme from carrying out oxidative chemistry. ***(b)*** The maximum parsimony phylogram of HRG-1 proteins from different species implemented using PHYLIP (v. 3.6).

Fig. S2: ZnMP fluorescence accumulation in *hrg-1* and *hrg-4* RNAi worms. Total mean fluorescence intensity of ZnMP was calculated in ≈ 50 worms from each RNAi treatment by epifluorescence microscopy and SimplePCI software. Each data point represents the mean ± SEM and the results are representative of three separate experiments. All values are significantly different ($P<0.05$), as determined by using a one-way ANOVA with Student–Newman–Keuls multiple comparisons test.

Fig. S3. Loss of *hrg-1* affects on zebrafish erythropoiesis. (a) Whole mount *in situ* hybridization for *βe1-globin* mRNA in wild type and *hrg-1* MO2 morphants. Loss of *hrg-1* results in a failure to maintain embryonic erythroid cells. ***(b)*** Analysis of myelopoiesis in *hrg-1* morphant embryos. Myeloid cells were analyzed by whole mount *in situ* hybridization with myeloid-lineage markers, myeloperoxidase (*MPO*) and *L-plastin*, in wild type and *hrg-1* morphant embryos at 48 hpf. No significant differences in the expression of *MPO* and *L-plastin* mRNA were noted between wild type control and morphant embryos. Inset: higher magnification views of the *L-plastin* staining cells (arrows). ***(c)*** Analysis of thrombopoiesis in *hrg-1* morphant embryos. Morpholinos targeting *hrg-1* were microinjected into transgenic *Tg(CD41:GFP)* embryos in which thrombocytes (platelet-equivalent cells) were specifically tagged with green fluorescence protein (GFP). No significant differences in the number of circulating GFP+ thrombocytes (arrows) were appreciated in *hrg-1* morphants compared to wild type controls at 4 dpf. ***(d)*** Whole mount *in situ* hybridization for *pax2.1* mRNA. Loss of *hrg-1* in MO2 morphants results in a failure to form proper mid- and hind-brain structures.

Fig. S4: Quantitation of *hHRG-1* mRNA expression in human tissues and cell lines. Relative *hHRG-1* mRNA levels from Northern blots of human tissues ***(a)*** and cell lines ***(b)*** quantitated by ImageQuant v2.2. *hHRG-1* mRNA was normalized to β-actin as the loading control.

Fig. S5: Expression pattern of mammalian *HRG-1* in cultured cells. *(a)* Human HRG-1 mRNA levels were unaltered by heme or iron depletion in cultured HEK293 cell lines. Cells were either grown in basal growth medium or in the presence of heme-depleted medium (HD), 500 μM succinyl acetone (SA) to inhibit heme synthesis, and 100 μM desferroxamine (DFO) to chelate iron. After 14 h of heme/iron depletion, cells were exposed to either 50 μM heme or 100 μM iron-SIH for 3 h. Total RNA was

extracted from cells and processed for qRT-PCR using primers designed to amplify cDNA for *HRG-1*, heme oxygenase (*HMOX1*) and the transferrin receptor (*TfR1*). Gene specific fold induction was quantitated by normalizing to *GAPDH* as the loading control. (***, P < 0.001 and *, P < 0.05 between basal conditions and the indicated treatment). Mean values were calculated, and differences were compared by using a one-way ANOVA with a Student–Newman–Keuls multiple comparison test. ***(b)*** Mouse *Hrg-1* mRNA is not induced during erythroid maturation in cultured MEL cells. MEL cells (DS19 clones) were induced with 1.5 % DMSO (v/v) which results in appearance of *o*-dianisidine positive cells, a marker of hemoglobinization. *mHrg-1* mRNA was unaltered in MEL cells 72 h post differentiation compared with α*-globin* (*Hba-a1*), β*-globin* (*Hbb-b1*), and *Alas-2* mRNA. ***(c)*** Time-dependence of mouse *Hrg-1* mRNA expression as a function of erythroid maturation in MEL cells. *Hrg-1* expression does not vary during MEL cell differentiation. Total RNA obtained from MEL cells harvested at the specific time points after induction with DMSO were quantitated for *Hrg-1* mRNA expression using qRT-PCR and normalized to *Gapdh* as the loading control. Each data point represents the mean ± SEM and the results are representative of two separate experiments.

Fig. S6: Intracellular localization of human HRG-1. Confocal microscopy images of HEK 293 cells plated on coverslips and co-transfected with plasmids containing hHRG-1 tagged with ECFP at the C-termini (left) and the indicated organelle marker tagged with EYFP (right). (Bar = 20 microns).

Fig. S7: Flow cytometry reveals greater ZnMP fluorescence in MEL cells expressing hHRG-1. Dot plots with forward scatter (y-axis) and fluorescence intensity (x-axis) show higher percentage of fluorescence-positive cells (right gate with red arrow) in MEL cells stably expressing hHRG-1:HA compared to the control vector, indicating

that the exogenous hHRG-1 increases the efficiency of cellular ZnMP uptake/ accumulation.

Fig. S8: Currents from a *Xenopus* oocyte expressing CeHRG-4:HA. Currents elicited from a *Xenopus* oocyte injected with CeHRG-4:HA cRNA in the absence (left) and presence (right) of 20 μM hemin chloride. The oocyte was clamped at -60 mV and stepped to potentials ranging from -110 mV to +50 mV in 20 mV steps. Traces corresponding to steps to -110, --30, +10 and +50 mV are labeled. The horizontal dotted line represents the zero current base line, which also indicates the reversal potential. Scale bars shown are common to both traces. Note the shift in reversal potential indicated by the change in baseline between the two traces (from -30 mV in the absence of hemin to about -10 mV in the presence of hemin), as well as the pre-steady-state transient at high depolarization in the presence of heme.

Supplementary Methods

Biological materials, strains, cDNA Cloning, worm and cell culture. *C. elegans* strains [24] were grown either in liquid mCeHR-2 medium or on NGM agar plates spotted with *E. coli* OP50 or HT115(*DE3*) strains [25]. Synchronized L1 larvae were obtained by bleaching P_0 gravid worms grown in liquid mCeHR-2 medium supplemented with 1.5, 10 or 20 μM heme [26]. Hemin chloride, zinc mesoporphyrin IX and gallium protoporphyrin IX were purchased from Frontier Scientific, Inc. Plasmids for cloning and injections into worms were part of the Fire Vector Kit (Addgene). *C. elegans hrg-1* and *hrg-4* cDNA were cloned by reverse transcription of total RNA isolated from worms, and amplified by PCR using primers containing *Bam*HI and *Xho*I linkers, either with or without HA epitope tags. Primers designed to amplify worm ORFs were based either on Wormbase predictions or 5' and 3' RACE experiments. Human HRG-1 cDNA (GenBank accession number BC065033) was cloned by RT-PCR from HEK293 cells. The PCR products were ligated into plasmids pCDNA3.1(+) Zeo (Invitrogen) and pEGFP-N1 (Clontech) for expression in mammalian cells, pCS2 + for zebrafish experiments, or pT7TS for *Xenopus* oocyte expression. Cell lines were routinely cultured in basal growth medium composed of DMEM (GIBCO/BRL) and 10 % bovine serum supplemented with penicillin / streptomycin / glutamine. Transient transfections were performed either with Lipofectamine 2000 (Invitrogen) or FuGENE 6 (Roche). The following zebrafish strains were maintained and developmentally staged, as described [27]: wild type AB and Tü, and the transgenic line expressing green fluorescent protein under the CD41 promoter, Tg(CD41:GFP) [28]. *P* values for statistical significance were calculated by using a one-way ANOVA with Student–Newman–Keuls multiple comparison test by using INSTAT version 3.06 (GraphPad, San Diego).

RNA isolation and microarray analysis. Equal numbers of L1 larvae (F_1) were inoculated in mCeHR-2 medium with 4, 20 or 500 μM hemin chloride and grown at 20°C. Worms were grown for two synchronized generations and late L4 stage F_2 worms from all three heme conditions were harvested at the same developmental stage. Total RNA from three biological replicates were hybridized to Affymetrix *C. elegans* Whole Genome Arrays. Data from worms grown in mCeHR-2 medium with 4 and 500 μM hemin were compared to data from worms grown in 20 μM hemin. Microarray data were verified with the Robust Multichip Average Method (RMA, R package) and MAS 5.0, Affymetrix. As a starting point, we used an initial cut-off of ≥ 1.2 fold-change in mRNA expression for RMA and a ≥ 1.6 fold-change for MAS 5.0 which resulted in the identification of ≈370 genes (82 and 288). Amino acid sequences encoded by the 370 genes were used to determine protein topology (TMHMM 2.0, SOSUI), motifs (ELM, BLOCKS, Pfam), and pathway classification (KEGG). Putative human orthologs were identified by using the 370 worm protein sequences as queries for BLAST searches of the human genome databases and an E-value cut-off of 10^{-3}. Orthologs for *C. elegans hrg-1* were identified by BLAST searches in WormBase with the HRG-1 ORF. Multiple sequence alignment was performed by ClustalW (v. 1.83) and the maximum parsimony phenograms were created in PHYLIP (v. 3.6) using distance measures from the Jones-Taylor-Thornton matrix model and neighbor-joining method, rooted by designating *S. japonicum* and mouse *Hrg1* as the outgroup for CeHRG-1 orthologs and CeHRG-4 paralogs, respectively. The resulting tree was bootstrapped 1000 times.

cDNA synthesis, quantitative real-time PCR and RNA blotting. Primers spanning at least one intron for quantitative real-time PCR (qRT-PCR) were designed using Primer Express (Applied Biosystems) and Beacon designer 4 (Premier Biosoft) software. Two-step qRT-PCR was carried out to confirm the expression patterns of *hrg-1*, *hrg-4*, *hrg-5*,

hrg-6 and *gpd-2* (internal control). First strand cDNA was synthesized using 2 μg of total RNA using Superscript II First Strand cDNA synthesis kit (Invitrogen). PCR was performed using the iCycler iQ Real-time PCR Detection System (BioRad) with 0.12 U/μl Taq DNA polymerase, 40 nM fluorescein (Invitrogen), and SYBR Green I Nucleic Acid Gel Stain (Invitrogen) diluted 1:10,000 [29]. Quality of the PCR products was determined by dissociation curve analysis and gel electrophoresis. Each experiment was done in triplicate. Average C_T values were used for $2^{-\Delta\Delta Ct}$ calculations of relative fold changes in gene expression [30]. For RNA blot analysis, 10 μg of total RNA from worms was resolved on a 1.5 % formaldehyde agarose gel, transferred to a nylon membrane (Zeta Probe, BioRad) and probed with a ^{32}P-α-dCTP (Amersham Biosciences) labeled cDNA that was generated by random priming (Stratagene). The probes were hybridized to the membrane for 16 h in ULTRAHyb (Ambion), washed and analyzed after 48 h with a PhosphorImager (Molecular Dynamics).

***hrg-1::gfp* heme sensor and RNA interference assays.** *C. elegans hrg-1* putative promoter (≈3 kb upstream of ATG start codon) was cloned into the *Pst*I- *Apa*I sites of vector pPD95.67 to create a *hrg-1::gfp* transcriptional fusion. Transgenic lines were generated by microinjection of 50 ng/μl of the *hrg-1::gfp* plasmid into wild-type N2 worms along with pRF4 plasmid (*rol-6*) for positive selection of transformants [31]. The integrated transgenic strain (IQ6011) was generated using gamma radiation (2500 rads/5 min). *C. elegans hrg-1* and *hrg-4* ORFs were cloned into the *Pst*I- *Hind*III sites of the L4440 RNAi feeding vector and transformed into *E. coli* HT115(*DE3*). Equal numbers of IQ6011 synchronized F_1 L1 larvae, obtained from P_0 worms grown in mCeHR-2 medium plus 10 μM hemin, were placed on NGM agar plates containing 2 mM IPTG and spotted with RNAi feeding bacteria that had been grown in LB broth supplemented with either 5 or 25 μM hemin or no added hemin (0 μM) for 5.5 h. Worms were analyzed 96 h after RNAi feeding with a Leica MZF16A fluorescence stereoscope

and fluorescence intensity measurements were quantified with SimplePCI v 6.2 (Compix, Inc.). For analysis of ZnMP uptake, equal numbers of IQ6011 synchronized F_1 L1 larvae obtained from P_0 worms grown in mCeHR-2 plus 1.5 μM hemin, were exposed to the RNAi bacteria on NGM plates containing 1 mM IPTG for 60 h followed by exposure to 10 μM ZnMP for 16 h in mCeHR-2 medium containing 1.5 μM hemin. ZnMP fluorescence intensity was measured with a Leica DMIRE2 inverted microscope fitted with a Rhodamine filter and Nomarski optics and image intensity quantified with SimplePCI. GaPP toxicity measurements were performed by exposure of IQ6011 synchronized F_1 L1 larvae, obtained from P_0 worms grown in mCeHR-2 plus 1.5 μM hemin, to RNAi bacteria for 60 h followed by exposure to 1 μM GaPP in the continuous presence of RNAi bacteria on NGM agar plates to sustain knockdown. After 24 h of egg-laying, the P_0 mothers were discarded to prevent additional eggs from being laid. On day 5, the total number of surviving larvae and viable eggs that hatched was counted.

Immunological analysis and *in-vitro* translation. Plasmids were transiently transfected into cultured adherent monolayers of mammalian cells, and were harvested 48 h post-transfection by cell lysis in 20 mM HEPES, pH 7.4/0.5 % Triton X-100/150 mM NaCl supplemented with protease inhibitor cocktail set II (Calbiochem Corp.) on ice for 15 min, followed by centrifugation for 10 min at 16,000 X *g* at 4ºC. The Bradford (BioRad) method was used to determine protein concentration from all samples. For immunoblotting, lysates were mixed with Laemmli Sample Buffer containing either β-mercaptoethanol or 100 mM DTT without heat denaturation, resolved by SDS-PAGE, and transferred to nitrocellulose membranes for detection by either the SuperSignal West Pico or West Femto Chemiluminescence kits (Pierce) and horseradish peroxidase conjugated secondary antibody (Pierce). Linearized ORFs cloned into pcDNA3.1(+) zeo were transcribed and translated *in-vitro* in the presence of T7 polymerase, wheat

germ extract, and 22 μCi of [^{35}S]methionine and cysteine using a TNT kit (Promega), according to the manufacturer's instructions. The reaction product (1/5th) was resolved by SDS-PAGE, and the gels soaked in EnHance (Perkin Elmer) to enhance ^{35}S fluorography, dried, and exposed to a PhosphorImager (Molecular Dynamics). For immunofluorescence experiments, cells grown on glass coverslips were fixed in freshly made 4 % paraformaldehyde and permeabilized in 0.2 % Triton-X 100 as described [32]. Coverslips were mounted using ProLong Antifade (Molecular Probes) and analyzed with a PlanApo 60X oil immersion objective on a Leica DMIRE2 inverted microscope. For confocal microscopy studies, a laser scanning Zeiss LSM 510 confocal microscope equipped with Argon (458 and 488), HeNe (543 and 633) and a planApo 100X oil immersion objective was used. Rabbit polyclonal antibody against HA epitope (Sigma) or GFP (Qiagen) were used for immunoblotting or immunofluorescence experiments. In some experiments, cells grown on coverslips were incubated with Alexa 633 conjugated wheat germ agglutinin (Molecular Probes) for 5 min to label the plasma membrane. Organelle marker plasmids were generously provided by Dr. J. Lippincott-Schwartz.

Worm lysis and GFP measurements. IQ6011 was grown in mCeHR-2 medium supplemented with 1.5, 4, 20 or 500 μM hemin for two generations. Worms were harvested at 800 X *g* for 5 min and washed twice with M9 buffer. The final worm pellet was resuspended in M9 buffer with protease inhibitors and lysed with FastPrep-24 (MP Bio) in the presence of Lysing Matrix D beads for 60 s at 6.5 setting. The worm lysates were centrifuged twice at 16,000 X *g* for 30 min to remove worm debris and 700 μg of the total protein, as measured by the Bradford method, was used to quantify GFP fluorescence. Measurements were obtained at 20ºC using an ISS PC1 spectrofluorometer with 1 mm slit-width at a fixed excitation of 488 nm. Scanning emission spectra (500-600 nm) were obtained for each sample, and graphs were generated using the peak absorbance value of GFP at 506 nm.

Hemin-agarose pull-down assays. Transfected HEK293 cells were lysed for 30 min on ice in MS buffer (210 mM mannitol, 70 mM sucrose) and either 10 mM HEPES, pH 6.0 and 7.4, or 10 mM Tris, pH 8.5. The lysates were centrifuged at 100 X *g* for 5 min, and the post-nuclear supernatant was incubated for 30 min at room temperature in the presence of 300 nmol hemin-agarose, prepared as described [33]. The expression of individual proteins was first quantified by immunoblotting total cell lysates with HA antibodies and band intensities measured with Quantity One software, v. 4.5 (BioRad). Equivalent amounts of target protein, corresponding to 60 µg of HRG-1 proteins or 360 µg of hZIP4 cell lysates, were mixed with untransfected HEK293 cell lysates to obtain 500µg of total protein that was used for binding. The binding reaction mixture was centrifuged at 800 X *g* for 3 min, and the resulting agarose pellets were washed three times with 1 ml of wash buffer (150 mM NaCl, 1 % NP-40, and 50 mM Tris-HCl, pH 8.0). The final pellets were incubated with 8 M urea and Laemmli sample-loading buffer containing 100 mM DTT and frozen for 1 h at -80ºC to elute the bound proteins. Samples were thawed, briefly vortexed, and directly loaded on a 12 % SDS/PAGE. Resolved proteins were transferred to nitrocellulose membranes and processed for chemiluminescence detection. Band intensity measurements showed 300 fold less binding of hZIP4 to hemin-agarose compared to either HRG-4 or HRG-1.

Heme / iron depletion and MEL cell hemoglobinization studies. HEK293 cells were treated with heme-depleted medium (DMEM, 10 % heme-depleted FBS, 1% PSG, 0.5 mM succinyl acetone) for 20 h. Heme-depleted serum was generated by treatment with 10 mM ascorbic acid [34]. For iron chelation, 100 µM desferroxamine (Sigma) was added to the cells 6 h after addition of the heme-depleted medium. After 14 h incubation, the heme-depleted medium was replaced with medium containing DMEM, 10 % heme-depleted FBS, 1 % PSG, 0.5 mM succinyl acetone, and either 50 µM heme or 100 µM Fe-SIH and allowed to incubate for an additional 3 h. A 50 µM heme-replete medium

was generated by mixing 10 mM hemin chloride and 1 mg/ml BSA stock solution with tissue culture medium and incubated overnight at 4ºC. For iron stock solution, 5 mM ferric citrate was mixed with 5 mM SIH (salicylaldehyde isonicotinoyl hydrazone) in 1:2 ratio to generate Fe-SIH [35]. Cells were washed once with PBS, and total RNA was extracted using Trizol. Extracted RNA samples were treated with TurboDNase (Ambion). Total RNA (2 µg) from each sample was used for cDNA synthesis (iScript cDNA synthesis kit, BioRad). qRT-PCR was performed using primers for hHMOX1, hTfR1 and hHRG1. Fold change was calculated using the $2^{-\Delta\Delta Ct}$ method. Primers: hHMOX1, sense 5'-ATGACACCAAGGACCAGAGC and anti-sense 5'-TAAGGACCCATCGGAGAAGC, hTfR1, sense 5'- TGAATTGAACCTGGACTATGAGAG and anti-sense 5'- CTGGAAGTAGCACGG AAGAAG, hHRG1, sense 5'-CTTCGTGGGCGTCCTCTTCTC and anti-sense 5'- CTTCGT GGGCGTCCTCTTCTC. MEL cells (DS19 clones) were cultured in DMEM, 10 % FBS, 1 % PSG, and 1% non-essential amino acids (Invitrogen). The cells were induced with 1.5 % DMSO. After 4 days of induction, the cells were harvested and RNA was isolated. For the time-course study, cells were harvested every 12 h for a 72 h period after induction with DMSO. The cell pellets for RNA extraction were quick frozen in Trizol. Total RNA was extracted from all samples and treated with DNase as per manufacturer's instructions. qRT-PCR was performed on cDNA synthesized (First strand cDNA synthesis kit, Invitrogen) using 2 µg of total RNA from each of the samples. Quantitative analysis was done using the $2^{-\Delta\Delta Ct}$ method. To generate stable clones in MEL cells, 20 µg of pcDNA3.1-Zeo plasmids was linearized with *Bgl*II and electroporated into 4 x 10^6 cells. Cells were subjected to 300 µg/ml of zeocin selection for 10 days 48 h post-electroporation. Individual zeocin-resistant clones were isolated and screened by immunoblotting with HA antisera to identify stably expressing cell lines.

Flow cytometry. MEL cells stably expressing HRG-1 were incubated with 5 μM ZnMP for 0, 15, 30, 45, and 60 min in uptake medium (25 mM HEPES, pH 7.4, 130 mM NaCl, 10 mM KCl, 1 mM $CaCl_2$, 1 mM $MgSO_4$ and 2.5 μM BSA) and the fluorescence intensity of ZnMP accumulated within the cells was measured by flow cytometry (BD FACS caliber) in the FL3 channel using forward and side scatter.

Zebrafish experiments. Whole mount *in situ* hybridization (ISH) was performed on wild type and *hrg-1* morphants with *βe1-globin*, *gata1* and *pax2.1* cDNA probes according to standard protocols [36]. Digoxigenin (DIG)-labeled antisense cRNA probes for myeloperoxidase (MPO) and L-plastin [37] were detected with nitro-blue tetrazolium/5-bromo-4-chloro-3-indolyl phosphate (NBT/BCIP). Live embryos at 48-72 hpf were stained for hemoglobinized cells with *o*-dianisidine as described [38]. For morpholino knockdowns and rescues with cRNA, two different splicing anti-sense morpholinos [39], targeting zebrafish *hrg-1* gene (GenBank BC053186.1), were synthesized by GeneTools (Philomath, OR). MO1 was complementary to the splice-donor site of exon2:intron2: 5'-CAGCCAAGGAATTACCTGATAATC-3'. A second morpholino, MO2, was complementary to the splice-acceptor site intron2:exon3: 5'-CCATAATGCCAAAACTCC TGAAAAA-3'. Injected and control embryos were fixed at 24 and 48 hpf for whole mount ISH and *o*-dianisidine staining. *C. elegans hrg1* was subcloned into pCS2+ vector and linearized for synthesis of 5'-capped cRNA using the SP6 mMessage mMachine kit (Ambion). Fertilized zygotes at the 1-cell stage from wild-type zebrafish were injected with empirically pre-determined concentrations of either 5 ng MO1 or 1.5 ng MO2. Rescue assays were performed by co-injecting 1.5 ng MO2 with 200 pg of *C. elegans hrg-1* cRNA. Injected embryos were allowed to develop to 2-3 days post-fertilization (dpf), then stained with *o*-dianisidine for hemoglobinized cells [38]. For RNA isolation and semi-quantitative RT-PCR, total RNA was isolated from embryos at 24, 48, and 72 hpf (Qiagen) and RNA integrity was confirmed by staining

with ethidium bromide for 18S/28S rRNA in a 1 % agarose gel. For semi-quantitative RT-PCR, first strand cDNA was generated using 1 µg total RNA, 200 U Superscript III reverse transcriptase (Invitrogen), and zebrafish *hrg-1* specific primers (available on request). Aberrant *hrg-1* mRNA spliceforms in morphants compared to control embryos were determined by RT-PCR, and the respective products resolved on agarose gels. Primers encompassing exon 4 were used as an internal control. Live *Tg(CD41:GFP)* control and morphant embryos were mounted in 2.5% methylcellulose. Fluorescence images were acquired with an Orca IIER CCD camera (Hamamatsu City, Japan) mounted on a Nikon microscope equipped with a 10X objective (NA 1.4). Electronic shutters and image acquisition were under the control of Metamorph software (Molecular Devices, Downington, PA).

Electrophysiological measurements in *Xenopus* oocytes. HRG ORFs were subcloned into the pT7TS vector and capped polyadenylated RNA transcribed from the T7 promoter using the mMessage mMachine kit (Ambion). Methods of *Xenopus* oocyte retrieval and their maintenance have been previously described [40]. RNA injection, two-electrode voltage clamp of *Xenopus* oocytes and data analysis were carried out as described [40], except that a Dagan TEV-200 amplifier was used and the data digitized at 0.1 - 1 kHz.

Supplementary Notes

[24] Fukushige, T., Hawkins, M. G., and McGhee, J. D., The GATA-factor elt-2 is essential for formation of the Caenorhabditis elegans intestine. *Dev Biol* **198** (2), 286 (1998).

[25] Stiernagle, T., in *WormBook*, edited by WormBook The *C. elegans* Research Community, doi/10.1895/wormbook.1.7.1, http://www.wormbook.org. (2005).

[26] Rao, A. U., Carta, L. K., Lesuisse, E., and Hamza, I., Lack of heme synthesis in a free-living eukaryote. *Proc Natl Acad Sci U S A* **102** (12), 4270 (2005).

[27] Westerfield, M., *The Zebrafish Book: A Guide for the Laboratory Use of Zebrafish (Danio Rerio)*. (Univ. of Oregon Press., Eugene, 1993).

[28] Lin, H. F. et al., Analysis of thrombocyte development in CD41-GFP transgenic zebrafish. *Blood* **106** (12), 3803 (2005).

[29] Ellestad, L. E. et al., Gene expression profiling during cellular differentiation in the embryonic pituitary gland using cDNA microarrays. *Physiol Genomics* **25** (3), 414 (2006).

[30] Livak, K. J. and Schmittgen, T. D., Analysis of relative gene expression data using real-time quantitative PCR and the $2^{-\Delta\Delta C}$T Method. *Methods* **25** (4), 402 (2001).

[31] Evans, T.C., in *WormBook*, edited by WormBook The *C. elegans* Research Community, doi/10.1895/wormbook.1.7.1, http://www.wormbook.org. (2005).

[32] Hamza, I., Prohaska, J., and Gitlin, J. D., Essential role for Atox1 in the copper-mediated intracellular trafficking of the Menkes ATPase. *Proc Natl Acad Sci U S A* **100** (3), 1215 (2003).

[33] Tsutsui, K., Affinity chromatography of heme-binding proteins: synthesis of hemin-agarose. *Methods Enzymol* **123**, 331 (1986).

[34] Zhu, Y. H., Hon, T., Ye, W. Z., and Zhang, L., Heme deficiency interferes with the Ras-mitogen-activated protein kinase signaling pathway and expression of a subset of neuronal genes. *Cell Growth & Differentiation* **13** (9), 431 (2002).

[35] Ponka, P., Borova, J., Neuwirt, J., and Fuchs, O., Mobilization of iron from reticulocytes. Identification of pyridoxal isonicotinoyl hydrazone as a new iron chelating agent. *FEBS Lett* **97** (2), 317 (1979).

[36] Hauptmann, G., Two-color detection of mRNA transcript localizations in fish and fly embryos using alkaline phosphatase and beta-galactosidase conjugated antibodies. *Dev Genes Evol* **209** (5), 317 (1999).

[37] Bennett, C. M. et al., Myelopoiesis in the zebrafish, Danio rerio. *Blood* **98** (3), 643 (2001).

[38] Iuchi, I. and Yamamoto, M., Erythropoiesis in the developing rainbow trout, Salmo gairdneri irideus: histochemical and immunochemical detection of erythropoietic organs. *J Exp Zool* **226** (3), 409 (1983).

[39] Morcos, P. A., Achieving targeted and quantifiable alteration of mRNA splicing with Morpholino oligos. *Biochem Biophys Res Commun* **358** (2), 521 (2007).

[40] Varshney, A., Kavitha, S., and Mathew, M. K., Modulation of voltage sensitivity by N-terminal cytoplasmic residues in human Kv1.2 channels. *Eur Biophys J* **31** (5), 365 (2002).

Category †	Heme		Total* genes	Orthologs § in humans
	4μM	500μM		
1	↑	↓	9	6
2	↑	↔	108	44
3	↓	↑	13	5
4	↓	↔	32	17
5	↑	↑	24	10
6	↓	↓	29	9
7	↔	↑	96	45
8	↔	↓	59	28
Total			370	164

↑ Upregulated, ↓ down-regulated, ↔ no change

† Gene expression profiles were categorized based on the fold changes relative to 20 μM heme samples.

* Summary of genes that showed change in their expression profiles in response to heme determined by MAS 5.0 and RMA methods.

§ Human orthologs were identified using BLAST with E-value ≤10^{-3}.

Rajagopal et al. Table S1

a

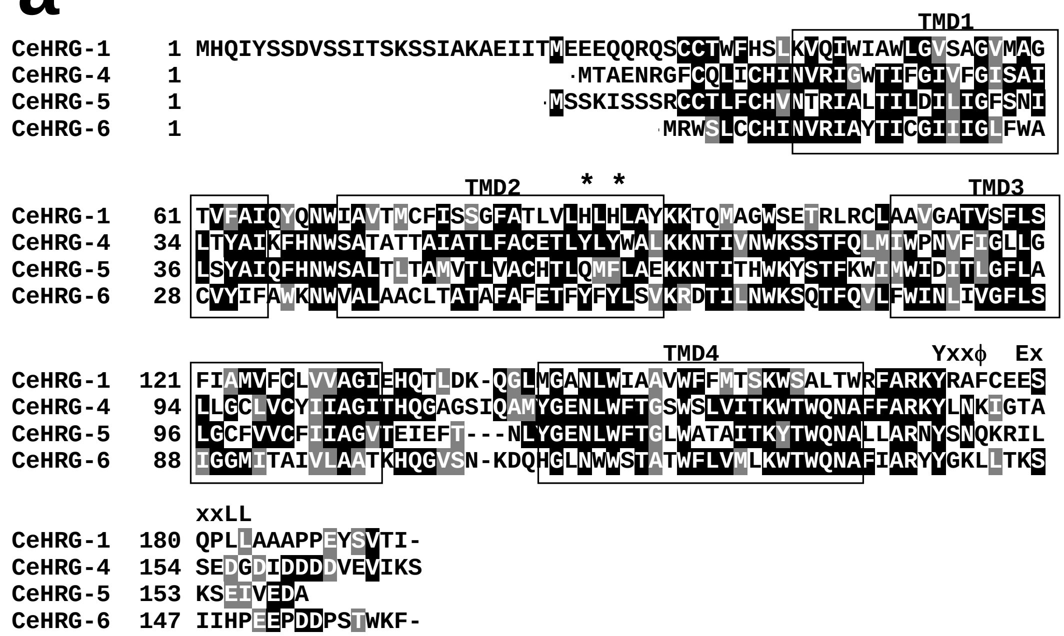

b

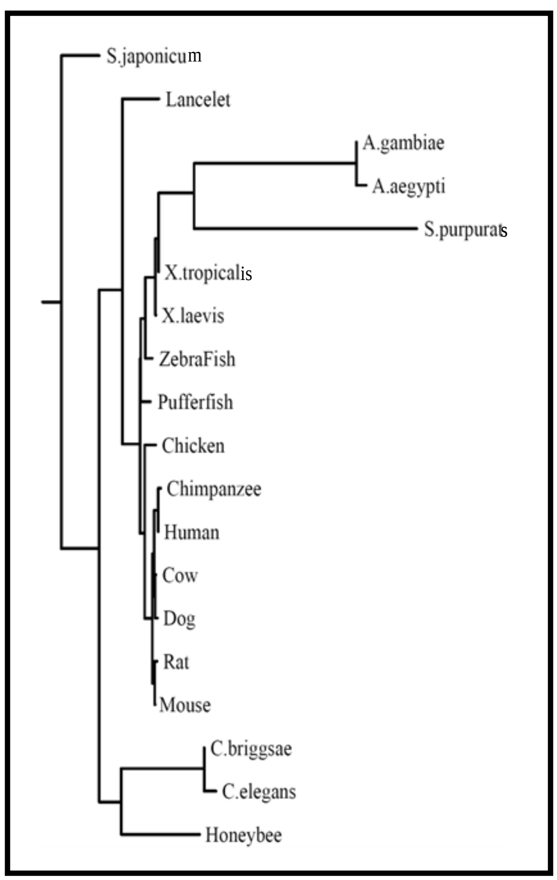

Rajagopal et al. Figure S1

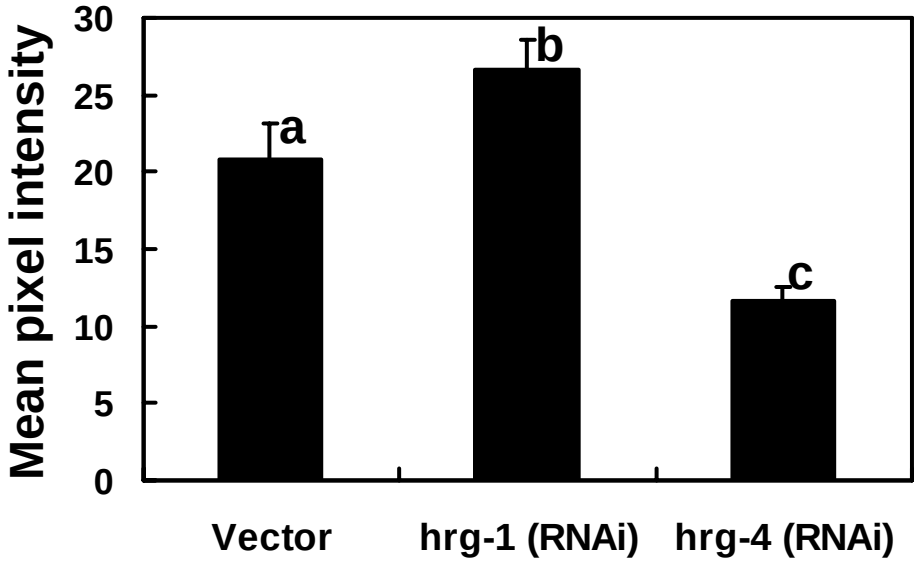

Rajagopal et al. Figure S2

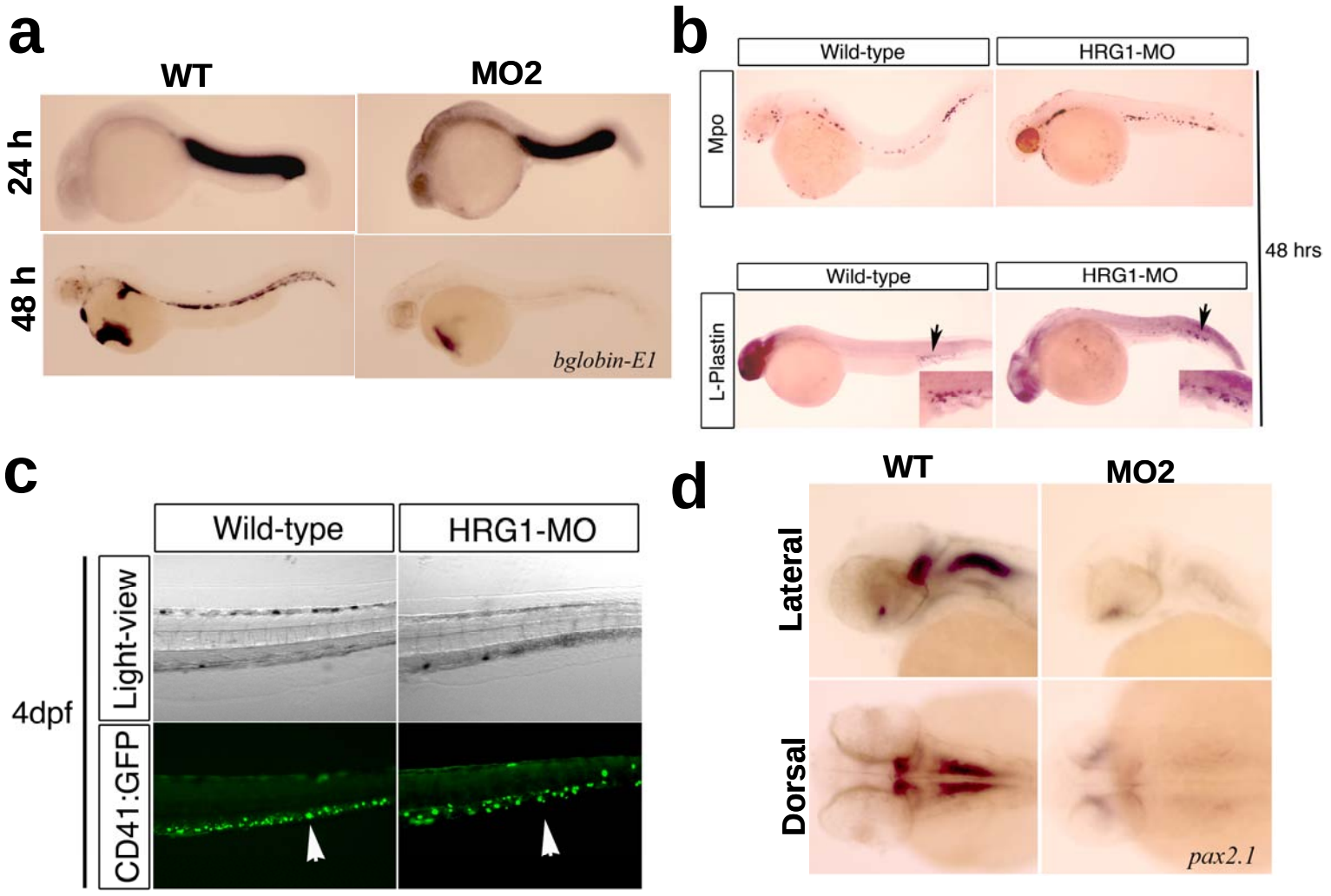

Rajagopal et al. Figure S3

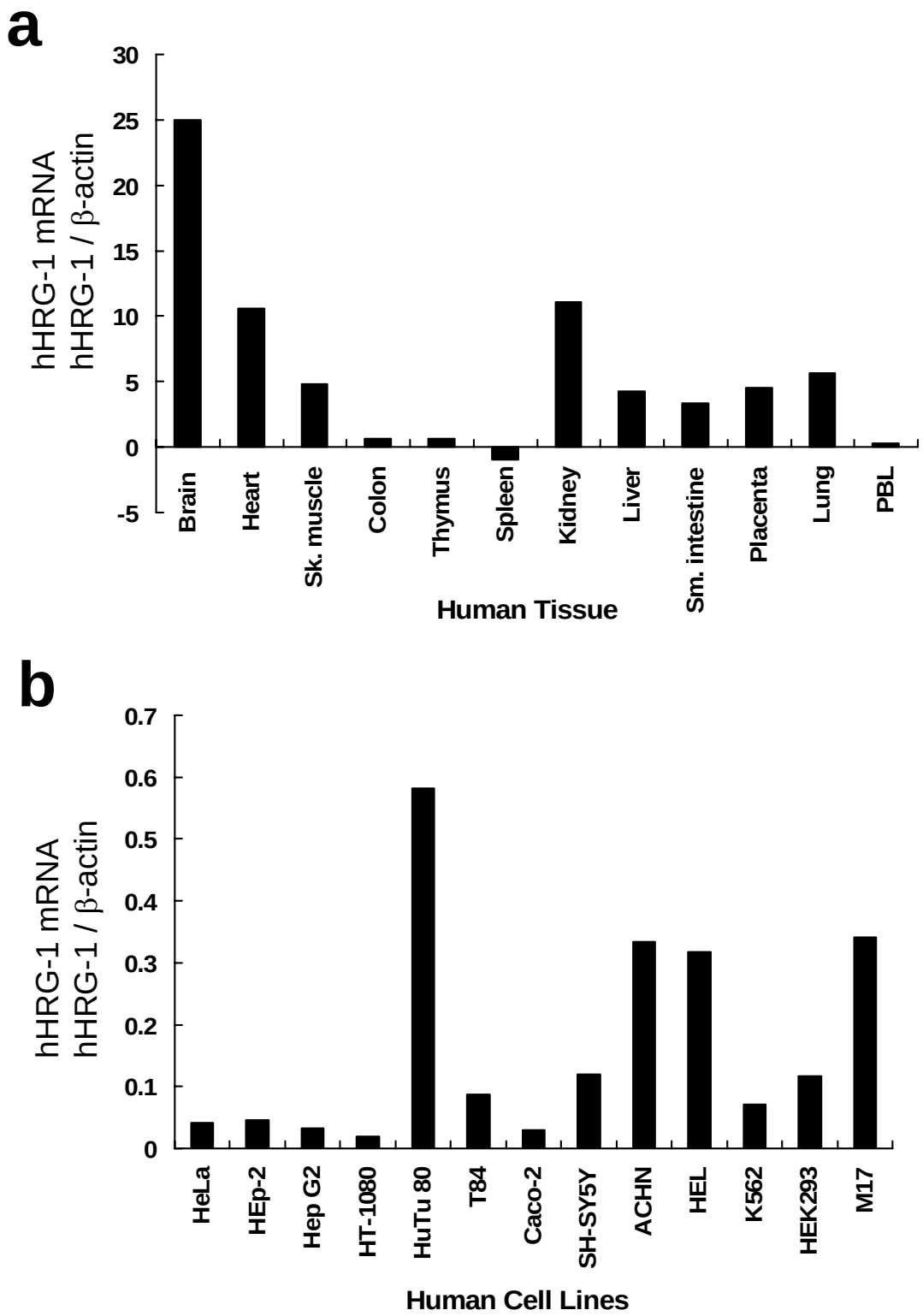

Rajagopal et al. Figure S4

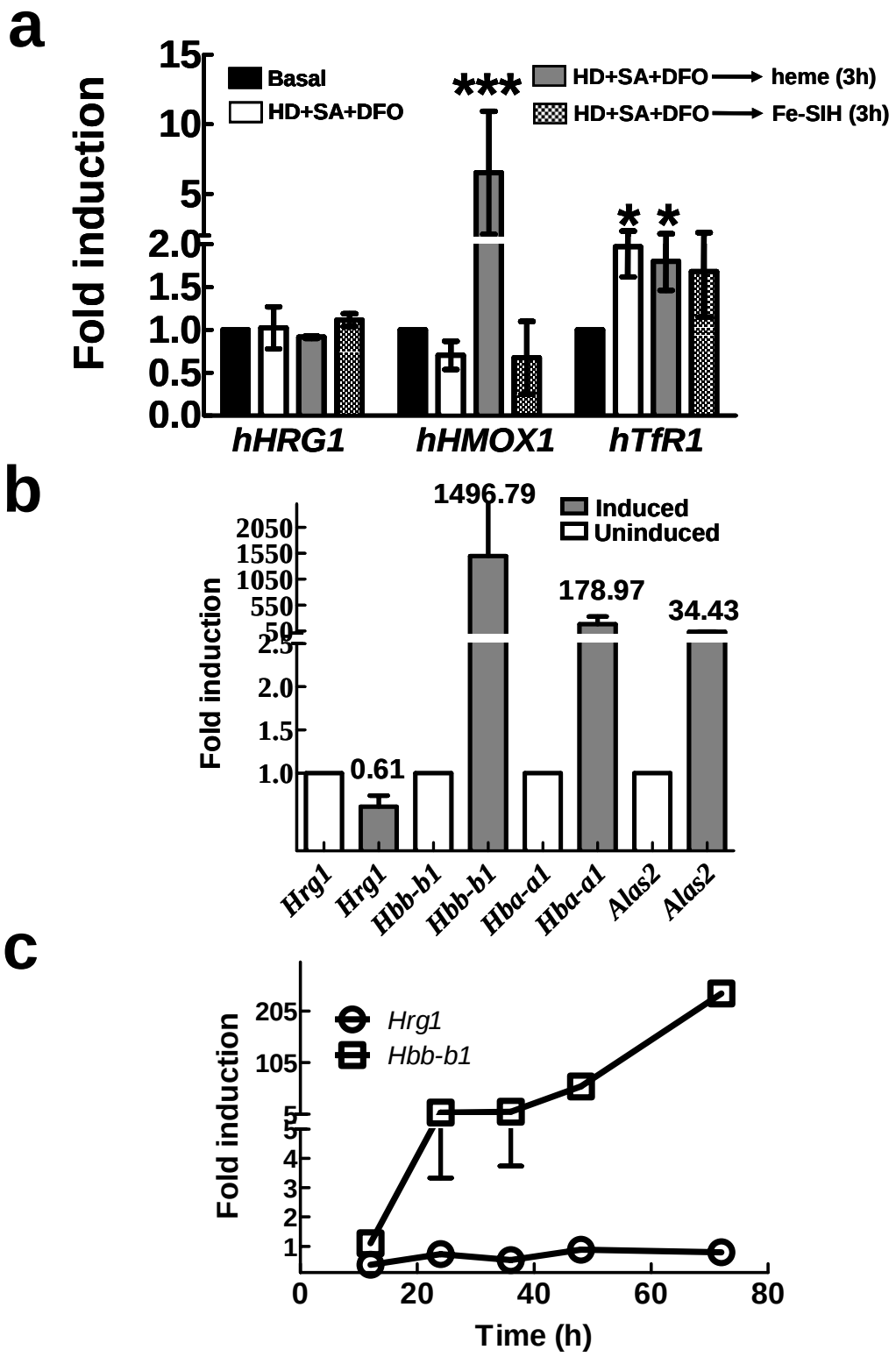

Rajagopal et al. Figure S5

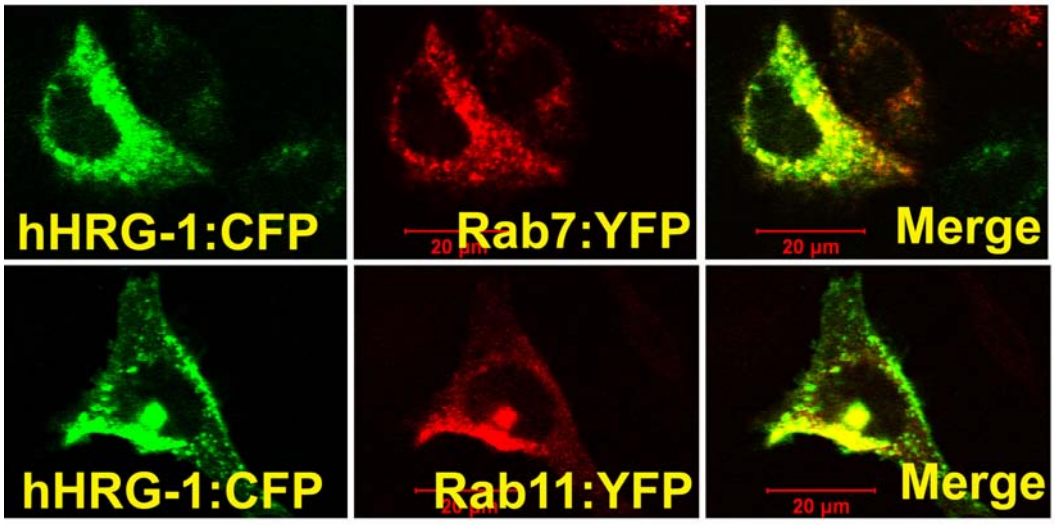

Rajagopal et al. Figure S6

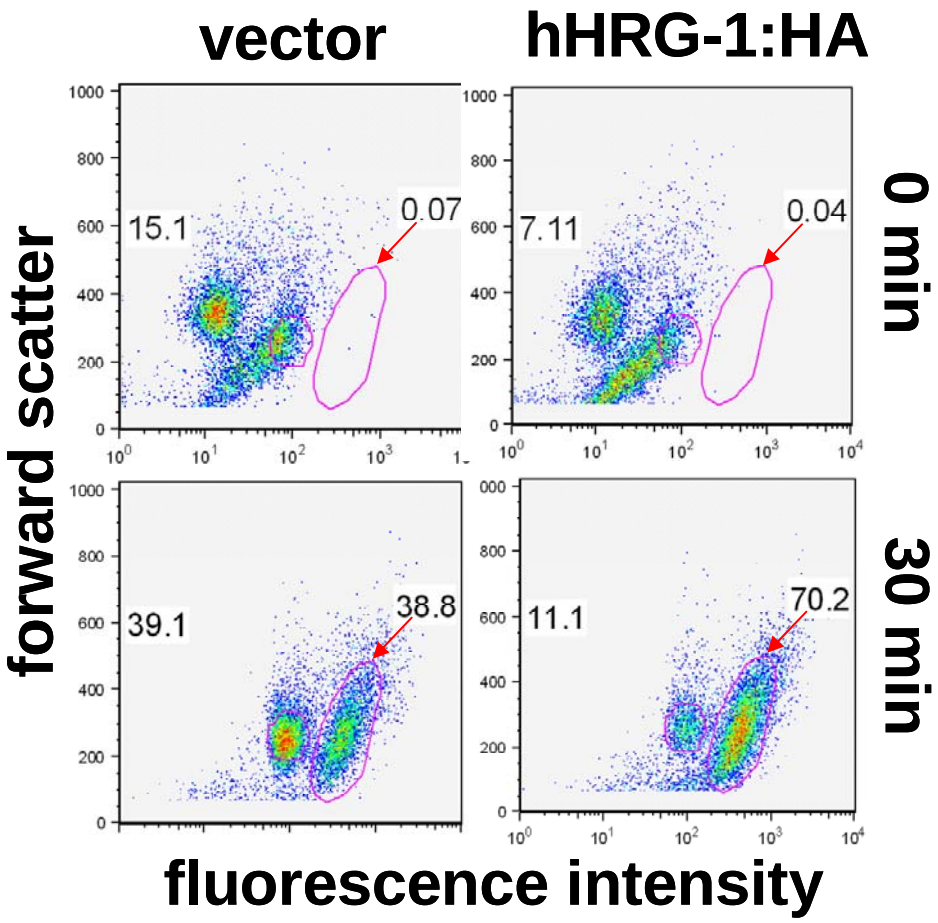

Rajagopal et al. Figure S7

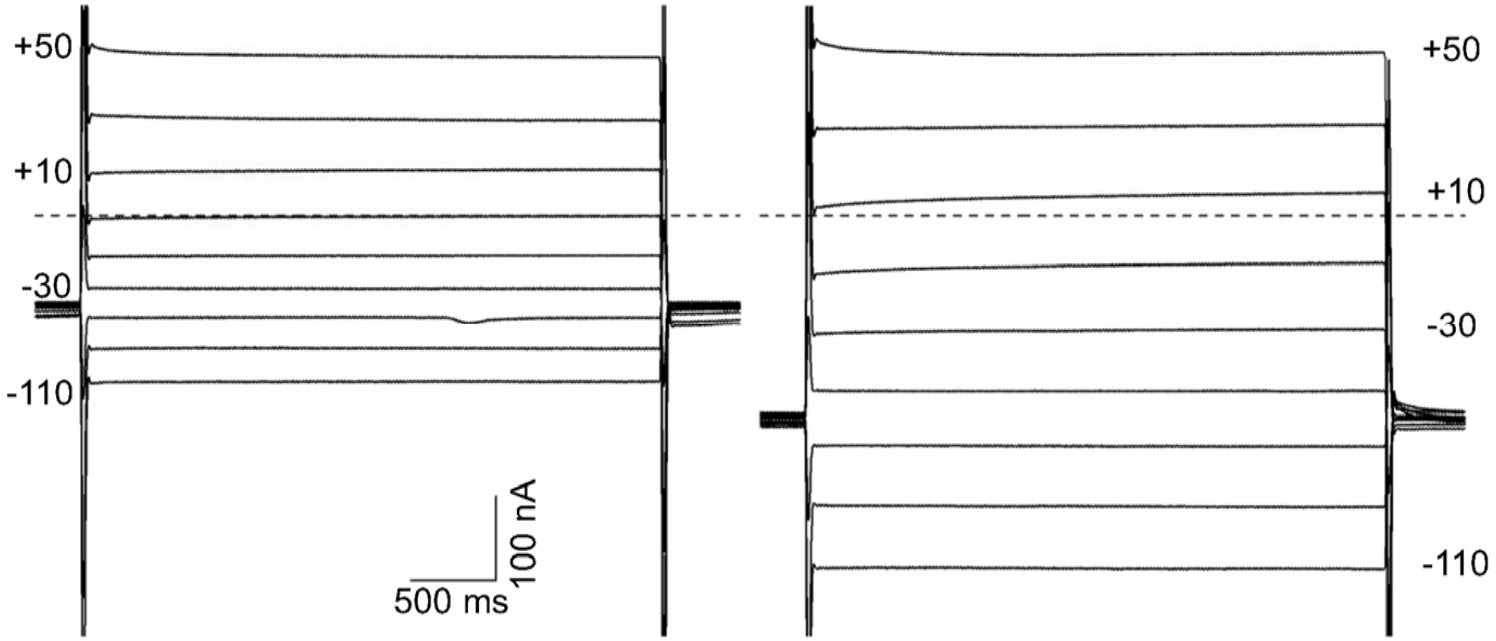

Rajagopal et al. Figure S8